

Supporting Information

Confined Interface Transformation of Metal Organic Frameworks for Highly Efficient Oxygen Evolution Reaction

Yueqing Wang,^[a] Lanling Zhao,^[b] Jizhen Ma^[a] and Jintao Zhang^[a]*

^[a] Dr. Y. Wang, Mrs. J. Ma, Prof. Dr. J. Zhang

Key Laboratory for Colloid and Interface Chemistry Ministry of Education

School of Chemistry and Chemical Engineering

Shandong University Jinan 250100 (P. R. China)

^[b] Dr. L. Zhao

School of Physics, Shandong University Jinan 250100 (P. R. China)

E-mail: jtzhang@sdu.edu.cn

1. Basic characterization of bulk MOF

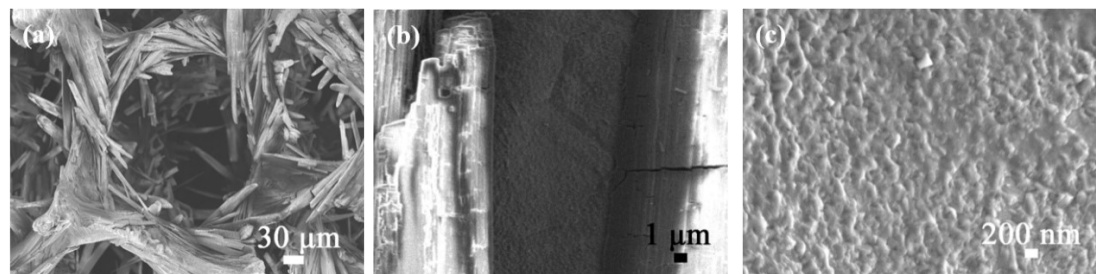


Figure S1. SEM images of bulk ZnMOF/NF.

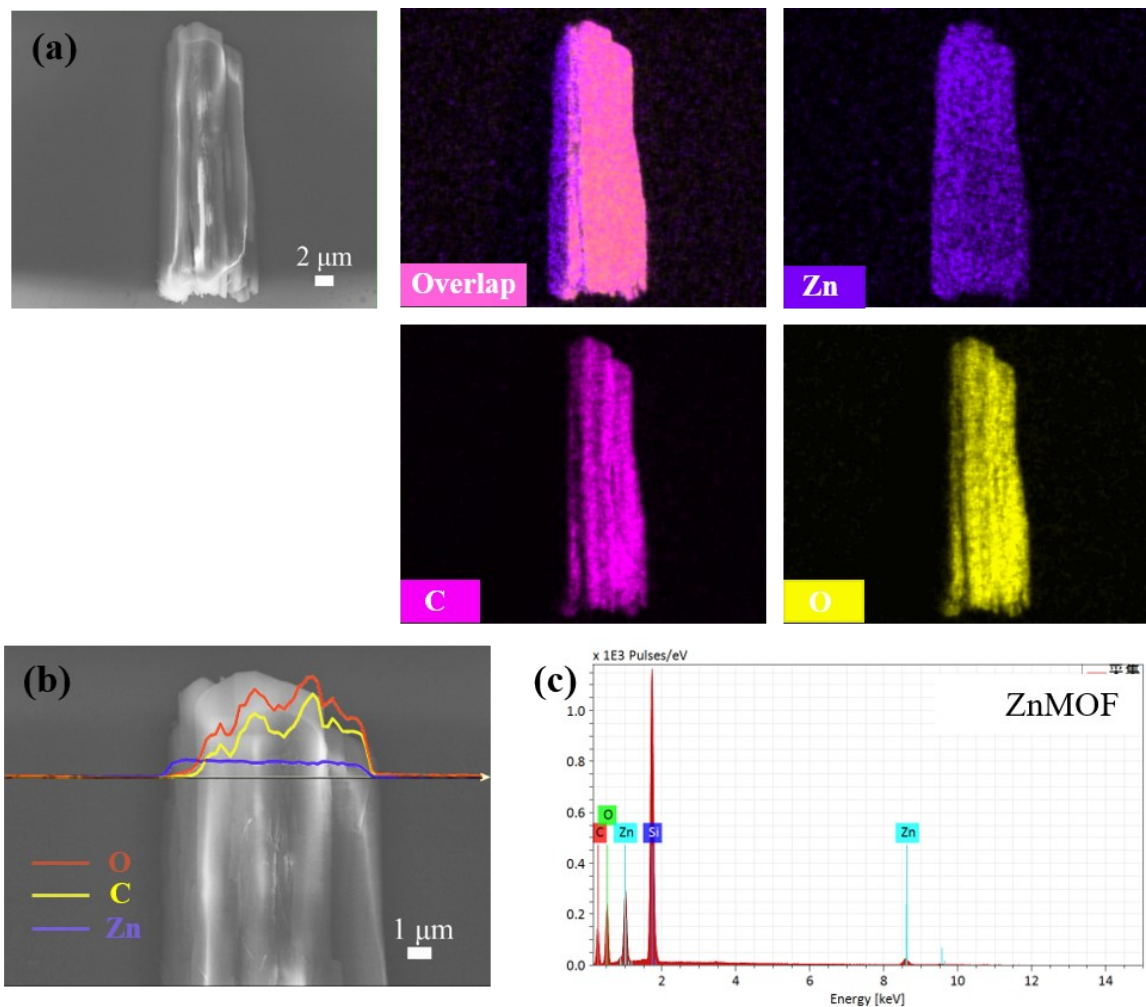


Figure S2. (a) EDS-mapping images of bulk ZnMOF, (b) linear scan profiles and (c) EDS spectrum of ZnMOF loaded on Si plate.

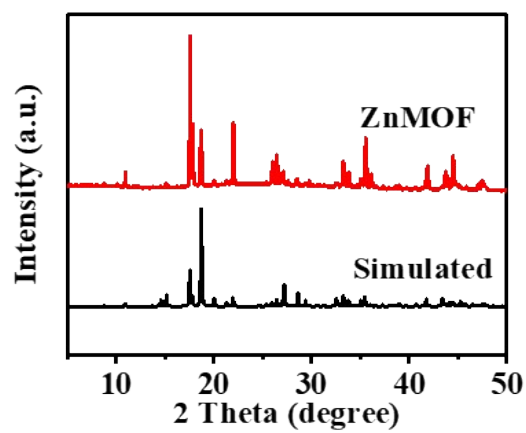


Figure S3. XRD pattern of ZnMOF and simulated XRD pattern of $\text{Zn}_3(\text{BTC})_2 \cdot 12\text{H}_2\text{O}$.

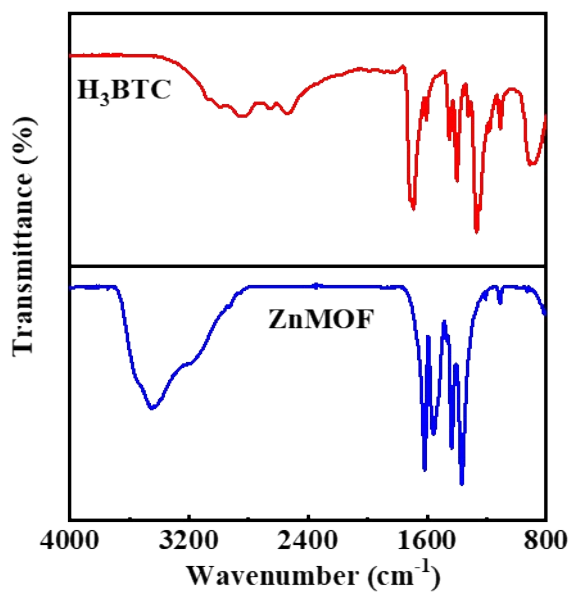


Figure S4. FTIR spectra of H₃BTC and ZnMOF.

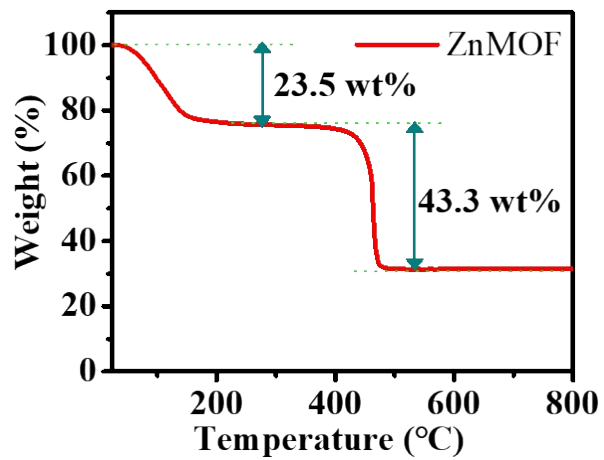


Figure S5. TGA profiles of ZnMOF in air.

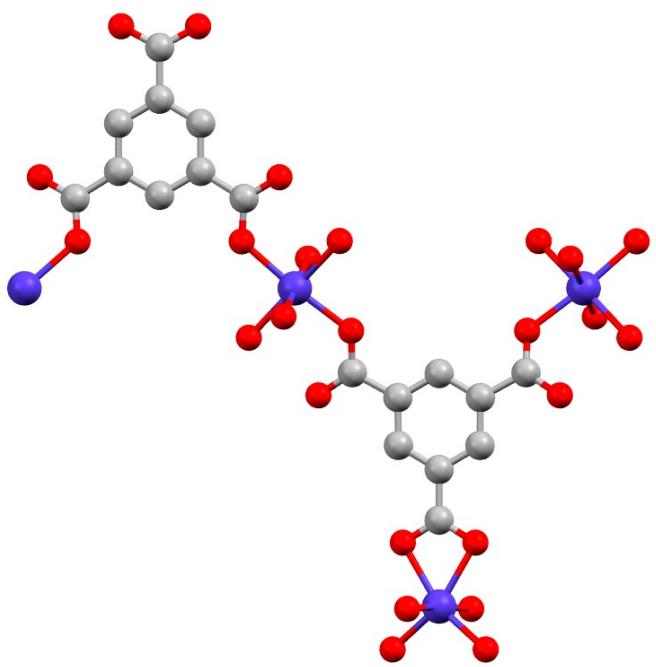


Figure S6. The monomeric unit of ZnMOF molecular structure.

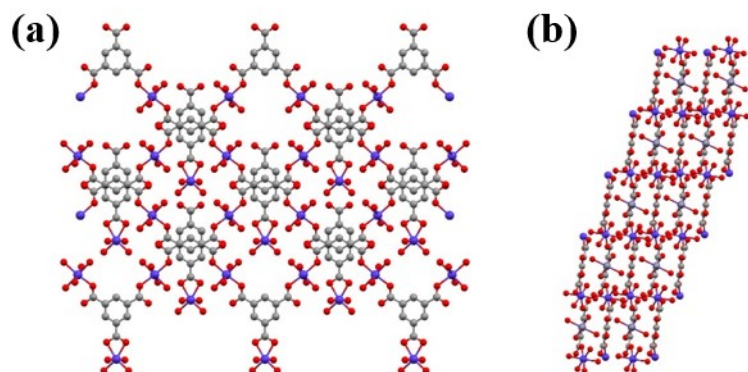


Figure S7. The atomic structure views of ZnMOF along c-axis (a) and b-axis (b).

2. Mass transport limited morphology evolution process

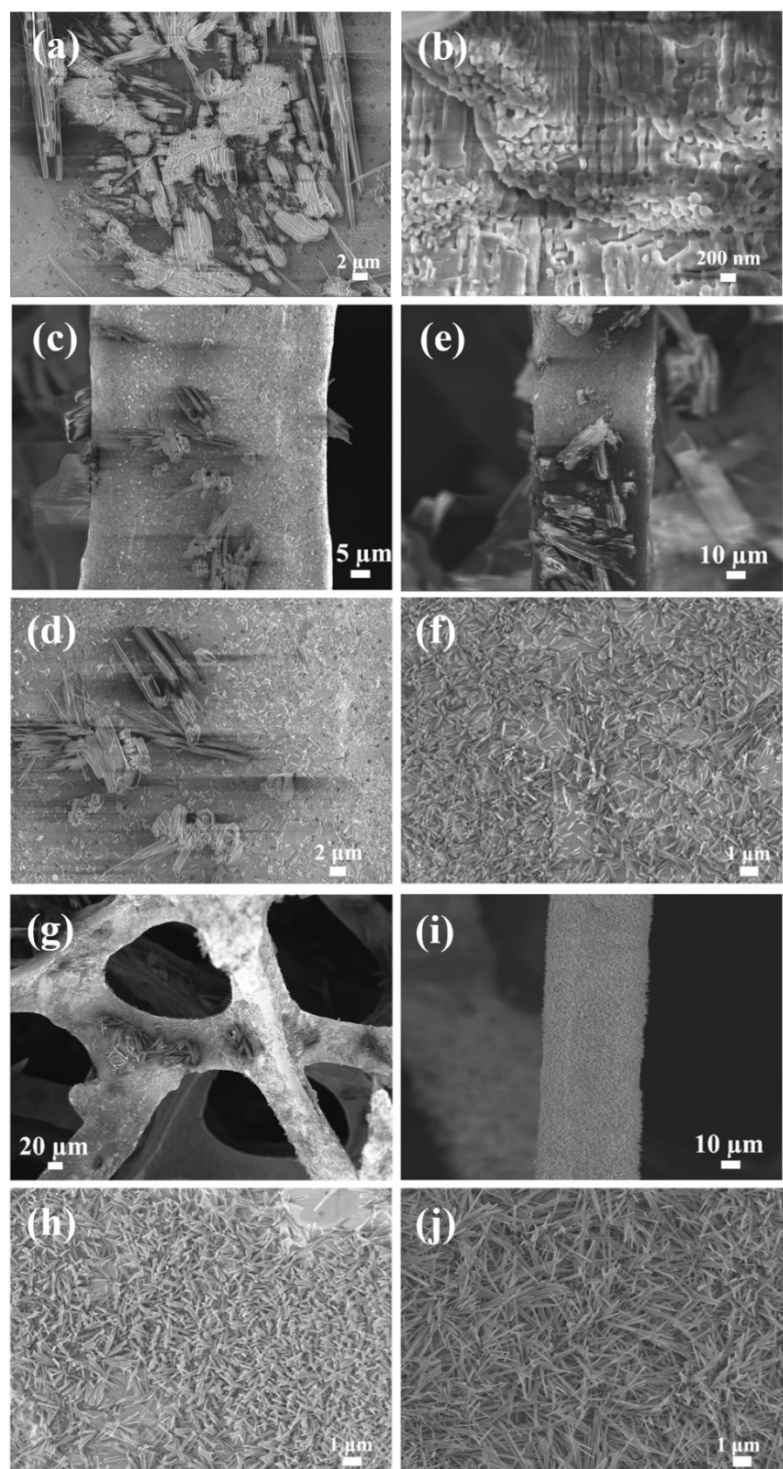


Figure S8. Time-dependent SEM images of ZnMOF immersed in static water for (a, b) 2 min, (c, d) 10 min (e, f) 30 min, (g, h) 2 h and (i, j) 5 h, respectively.

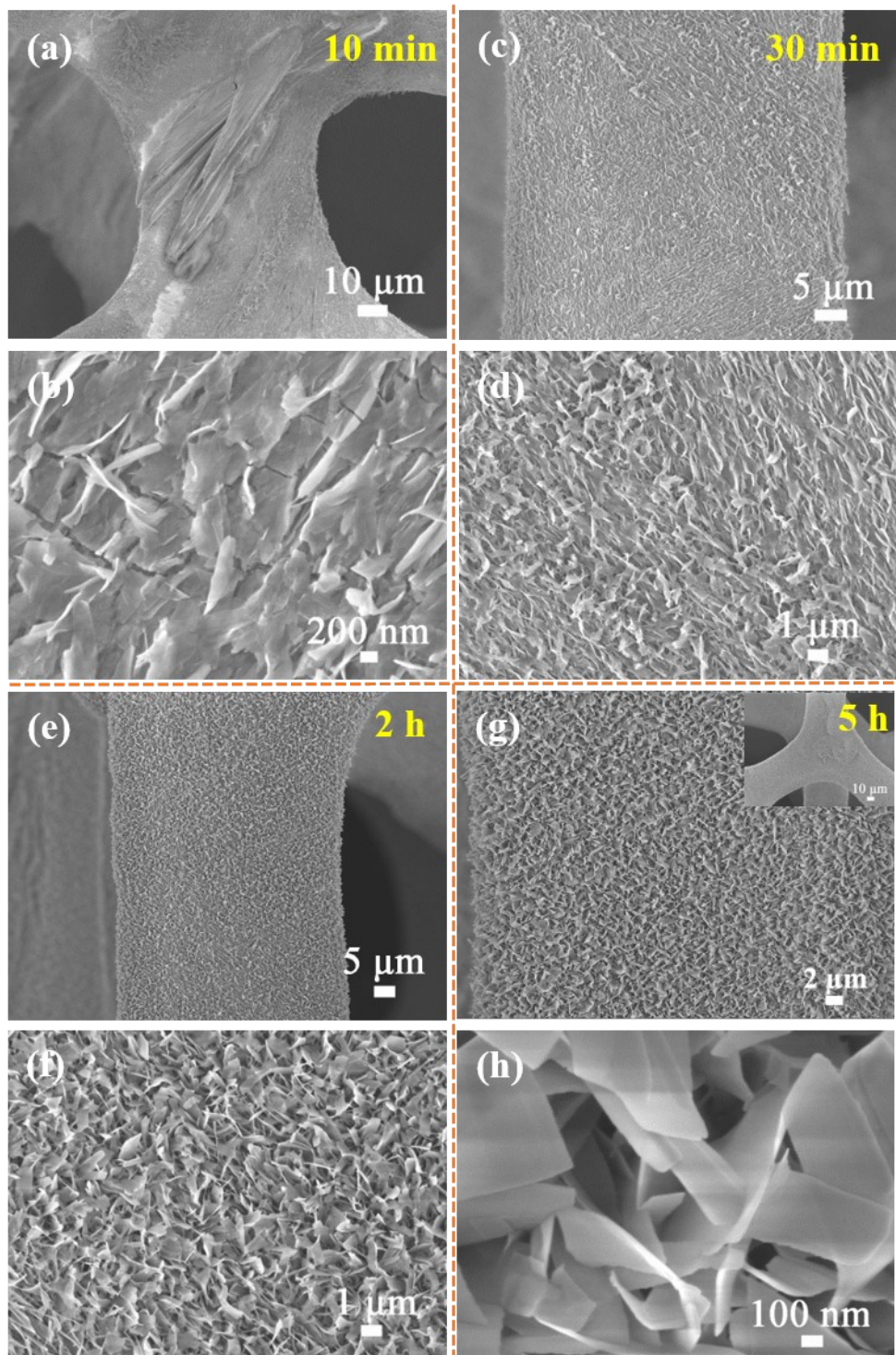


Figure S9. Time-dependent SEM images of ZnMOF immersed in water bubbled with N₂ for (a, b) 10 min, (c, d) 30 min (e, f) 2 h, and (g, h) 5 h, respectively.

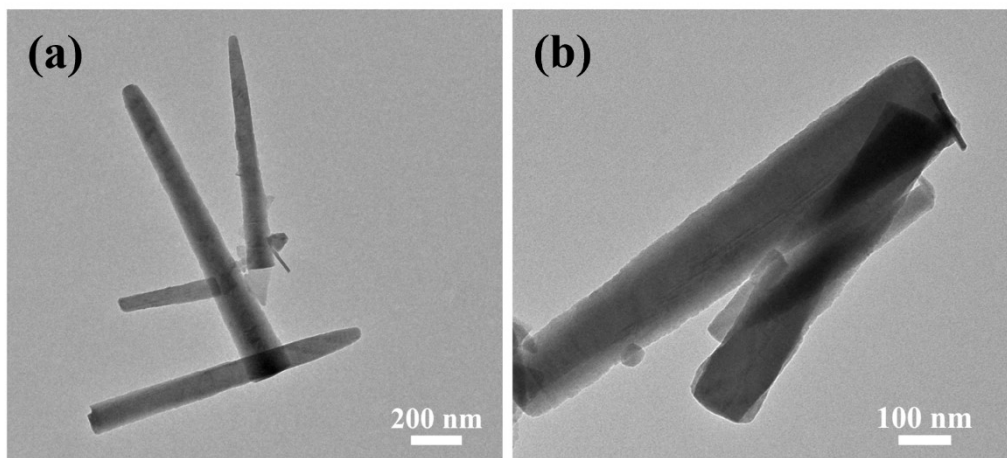


Figure S10. TEM images of ZnMOFS nanorods.

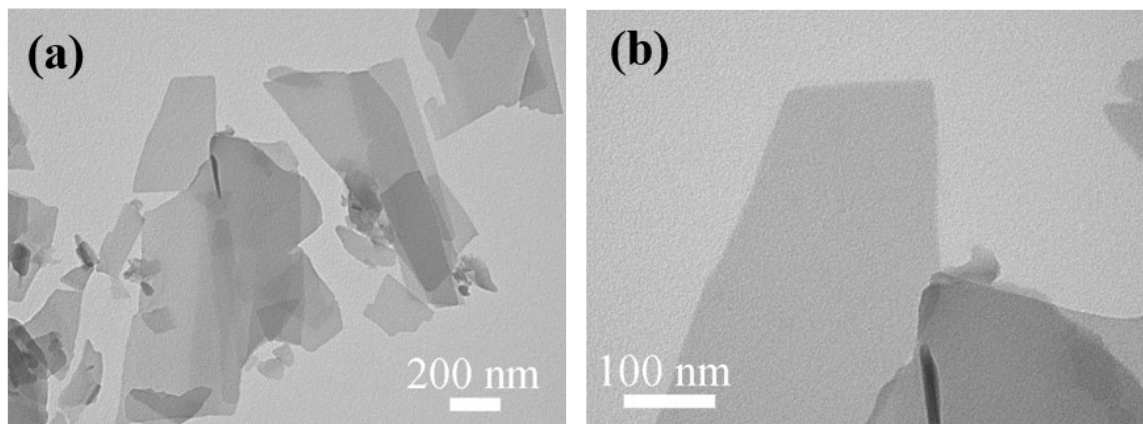


Figure S11. (a, b) TEM images of ZnMOFH.

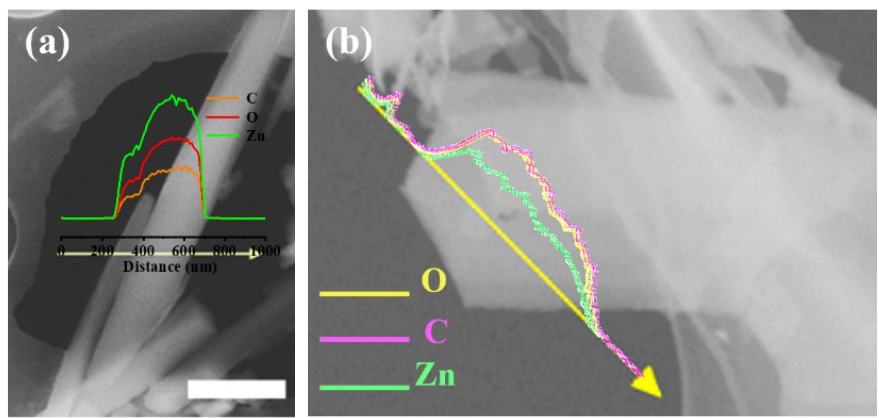


Figure S12. (a) Linear scan profiles of ZnMOFS nanorods, scale bar 500 nm and (b) ZnMOFH nanosheets.

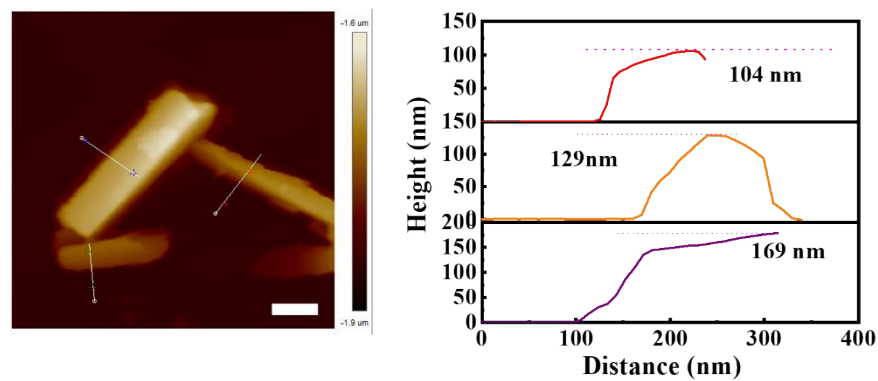


Figure S13. AFM image and the corresponding height profiles of ZnMOFS nanorods.

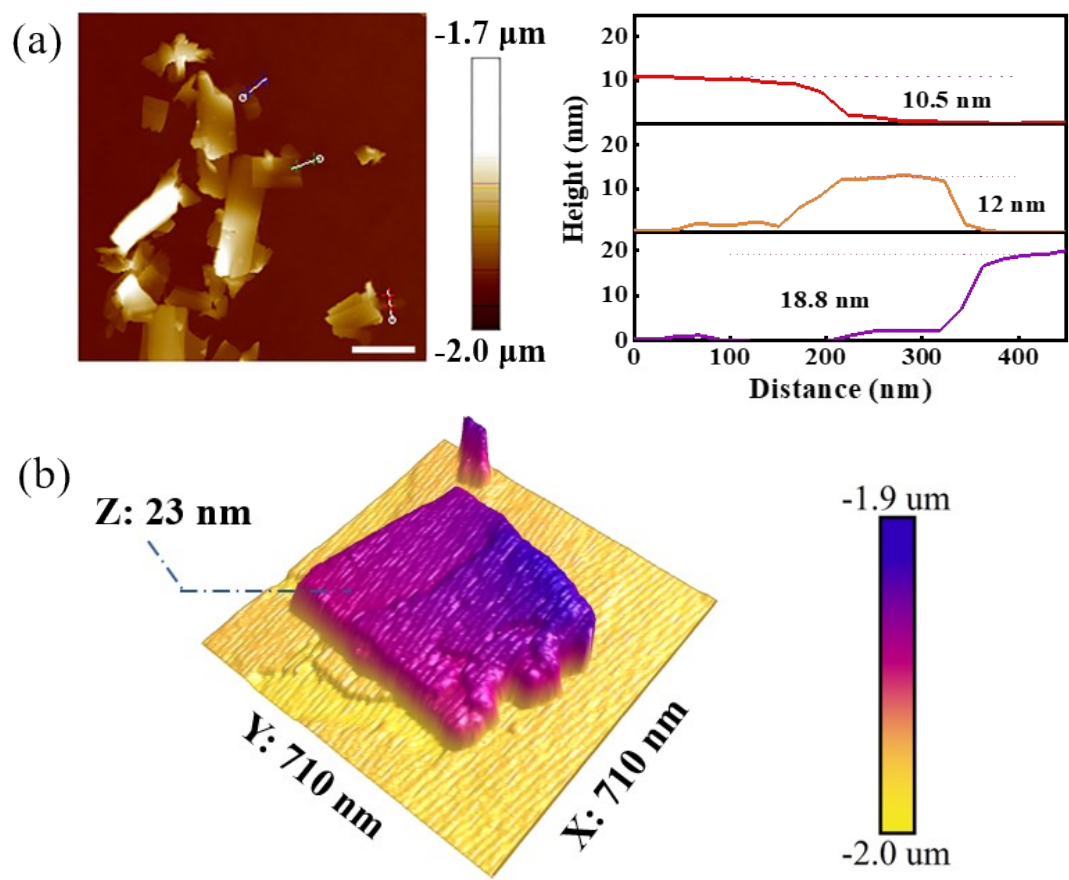


Figure S14. (a) AFM image and the corresponding height profiles of ZnMOFH. (b) AFM image of an individual ZnMOFH nanosheet.

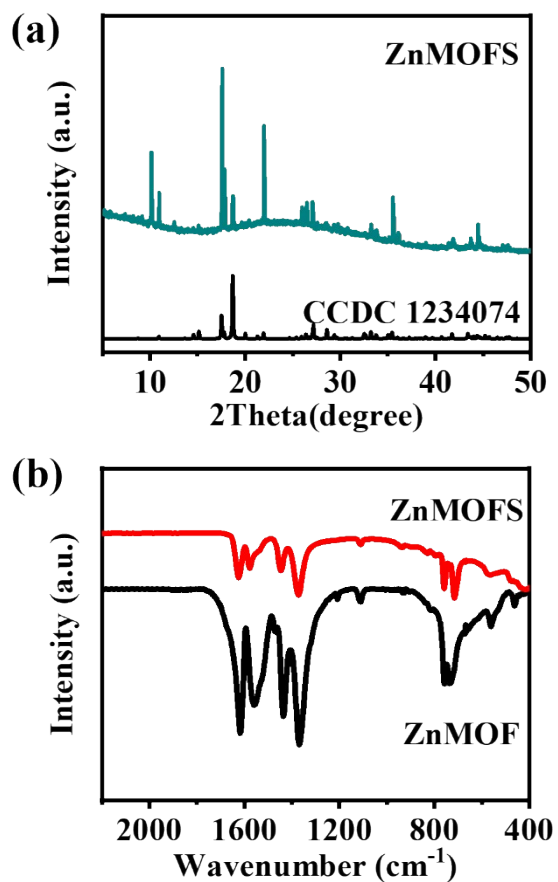


Figure S15. (a) XRD patterns and (b) FTIR spectra of ZnMOFS.

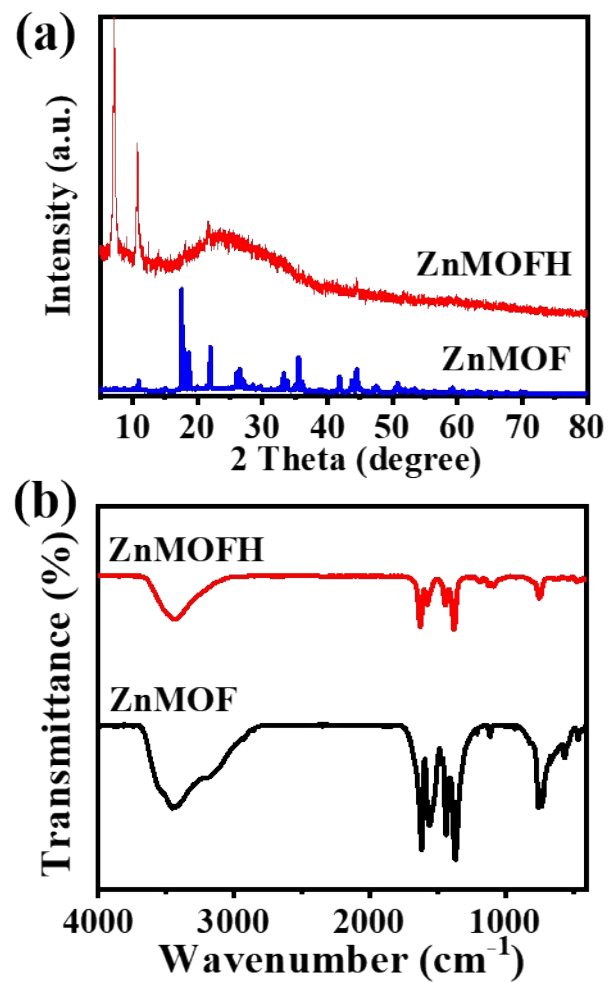


Figure S16. (a) XRD pattern, (b) FTIR spectra of ZnMOFH and ZnMOF.

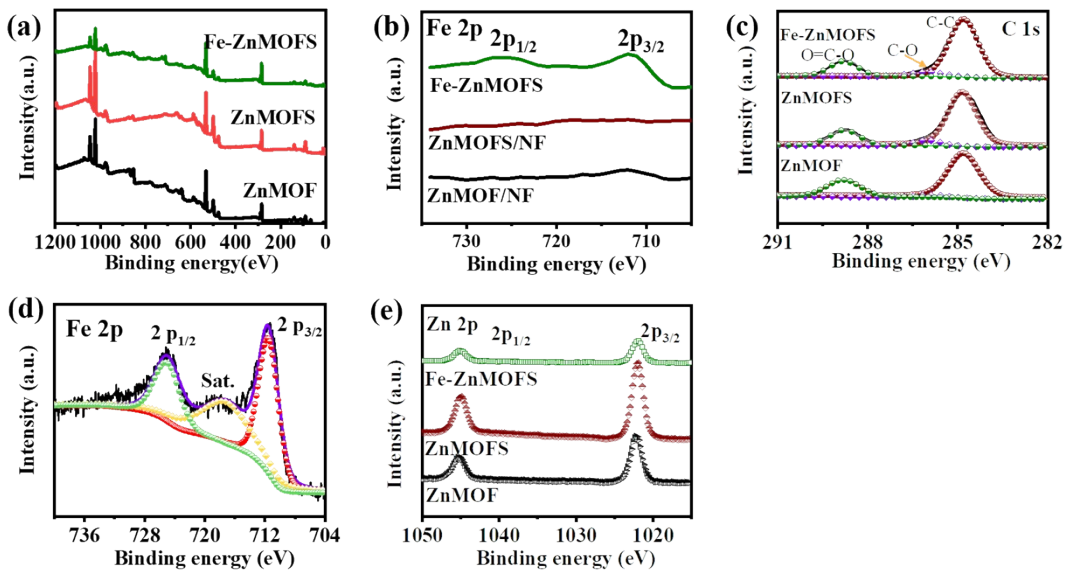


Figure S17. (a) XPS survey spectra of ZnMOF/NF, ZnMOFS/NF and Fe-ZnMOFS/NF. (b) Enlarged Fe 2p XPS spectra. High resolution XPS spectra of (c) C 1s, (d) Fe 2p and (e) Zn 2p.

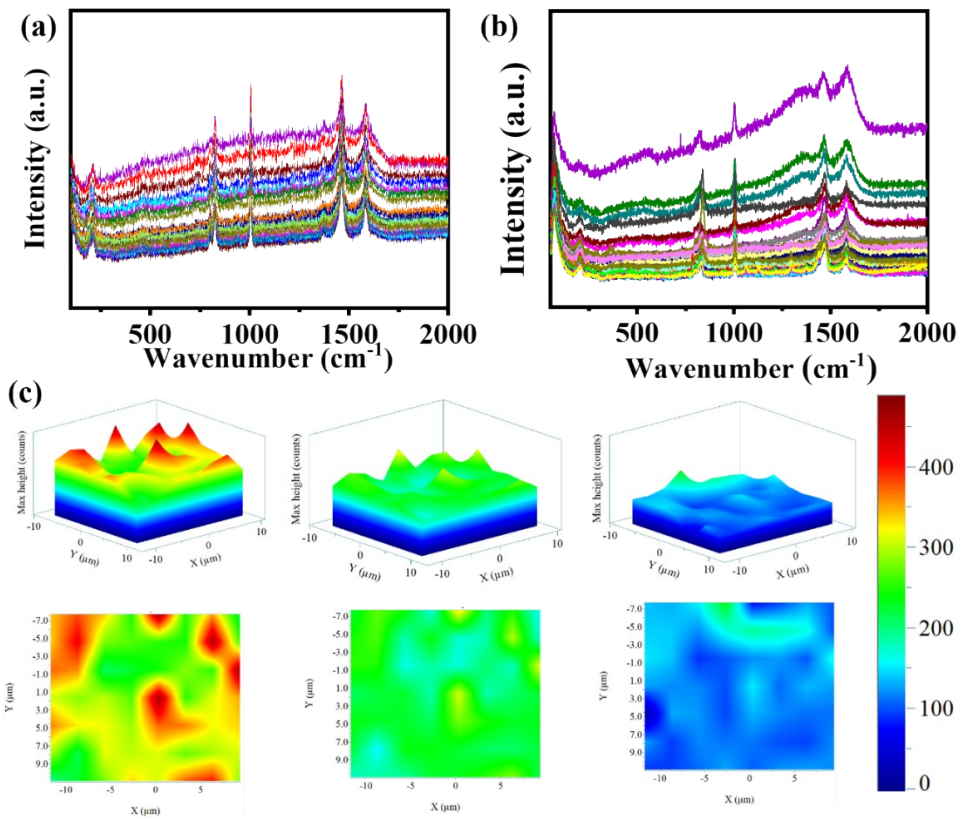


Figure S18. Raman spectra of ZnMOFS (a) and ZnMOFH (b). (c) Raman mapping images of ZnMOFH at the range of 960-1020, 1420-1520 and 1530-1620 cm^{-1} , respectively.

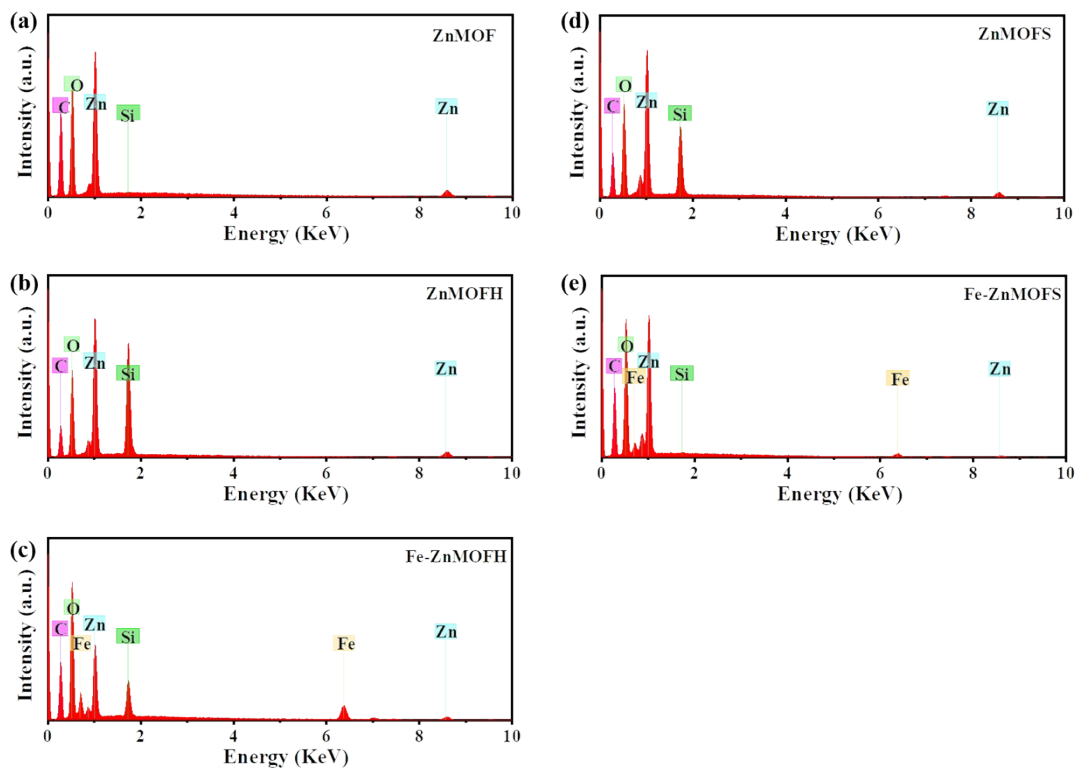


Figure S19. EDX spectra of diverse electrocatalysts.

3. Reaction mechanism

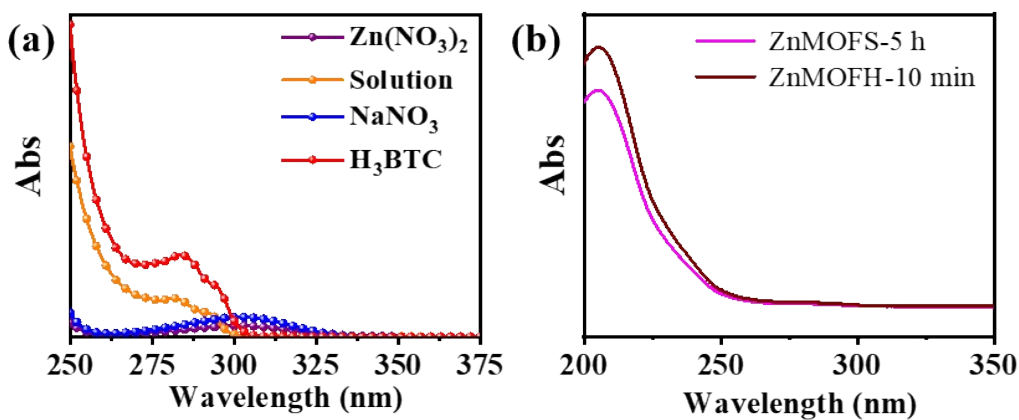


Figure S20. (a) UV-Vis spectra of H₃BTC solution, ZnMOF hydrolysis solution, and Zn(NO₃)₂ aqueous solution. (b) UV-Vis spectra of ZnMOF in static water for 5 h and in N₂ disturbance for 10 min.

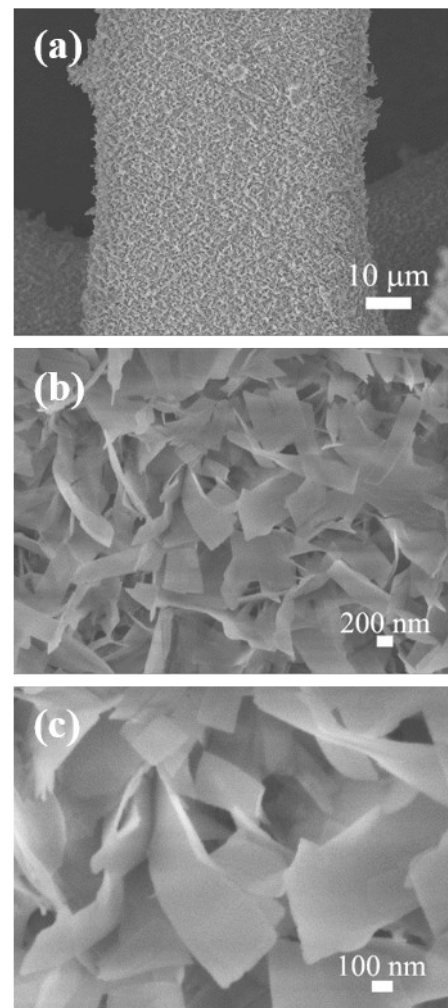


Figure S21. SEM images of ZnMOFH/NF with oxygen bubbling.

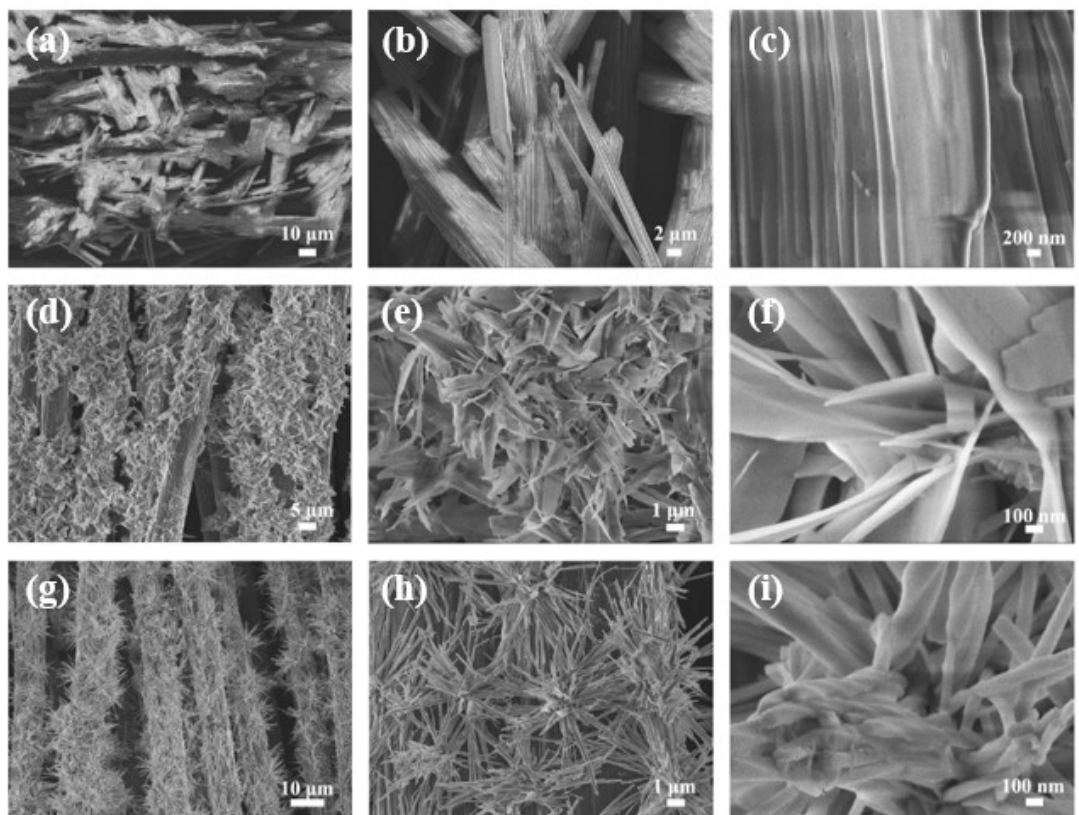


Figure S22. SEM images of ZnMOF/CC (a-c), ZnMOFH/CC (d-f) and ZnMOFS/CC (g-i).

4. Hybrid structure formation and electrochemical characterization

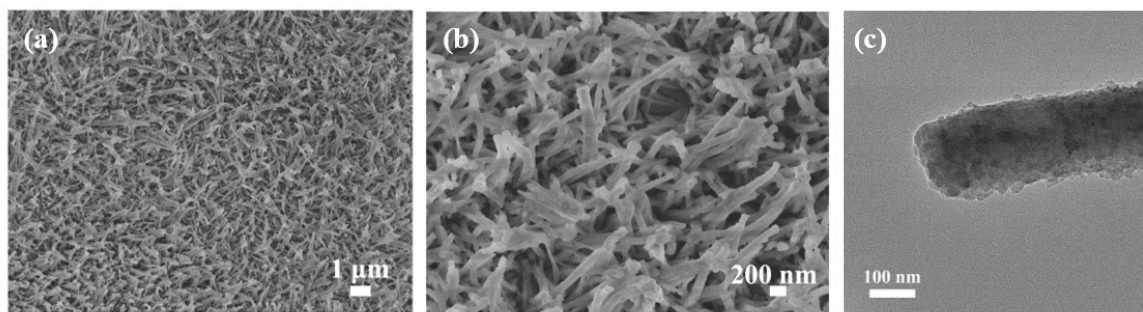


Figure S23. SEM (a, b) and TEM (c) images of Fe-ZnMOFS.

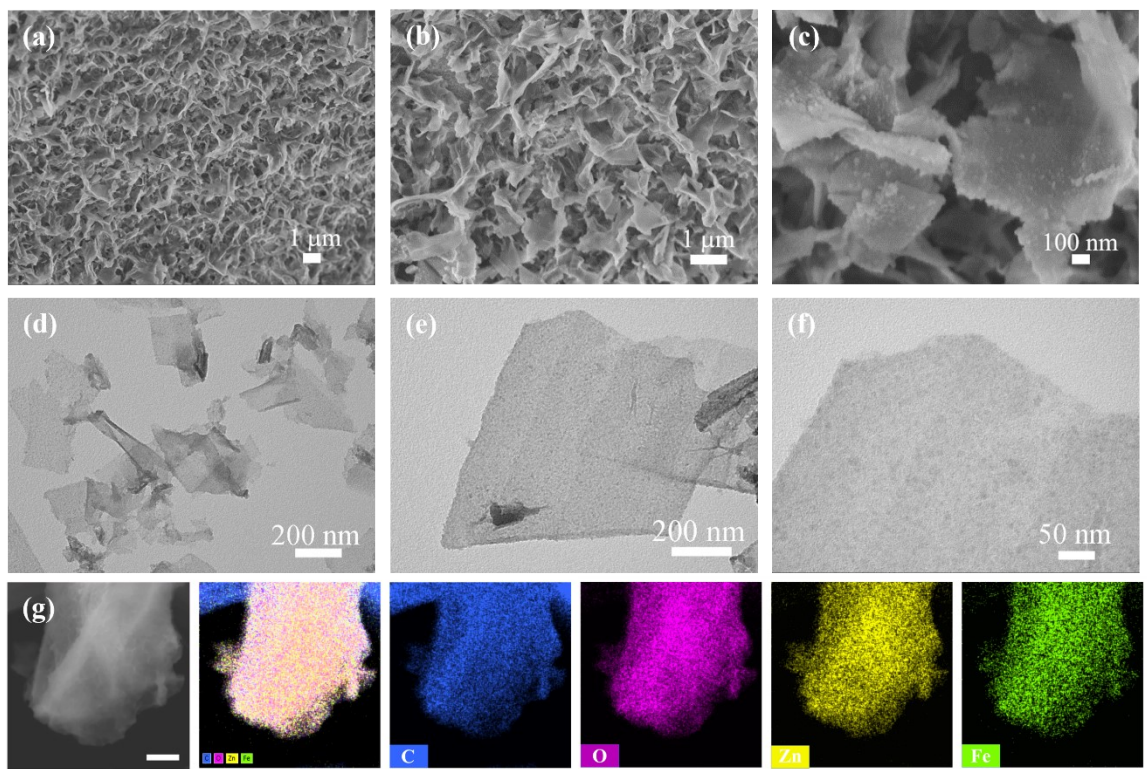


Figure S24. (a-c) SEM images and (d-f) TEM images of Fe-ZnMOFH. (e) EDS-mapping.

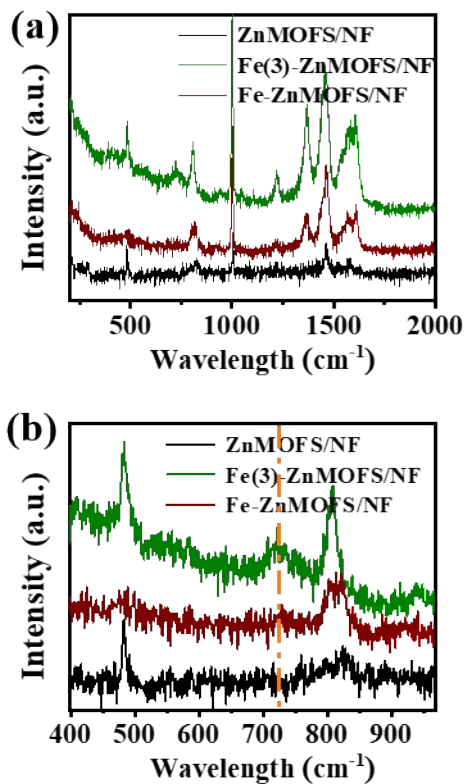


Figure S25. Raman spectra of ZnMOFS/NF, Fe-ZnMOFS/NF and Fe(3)-ZnMOFS/NF.

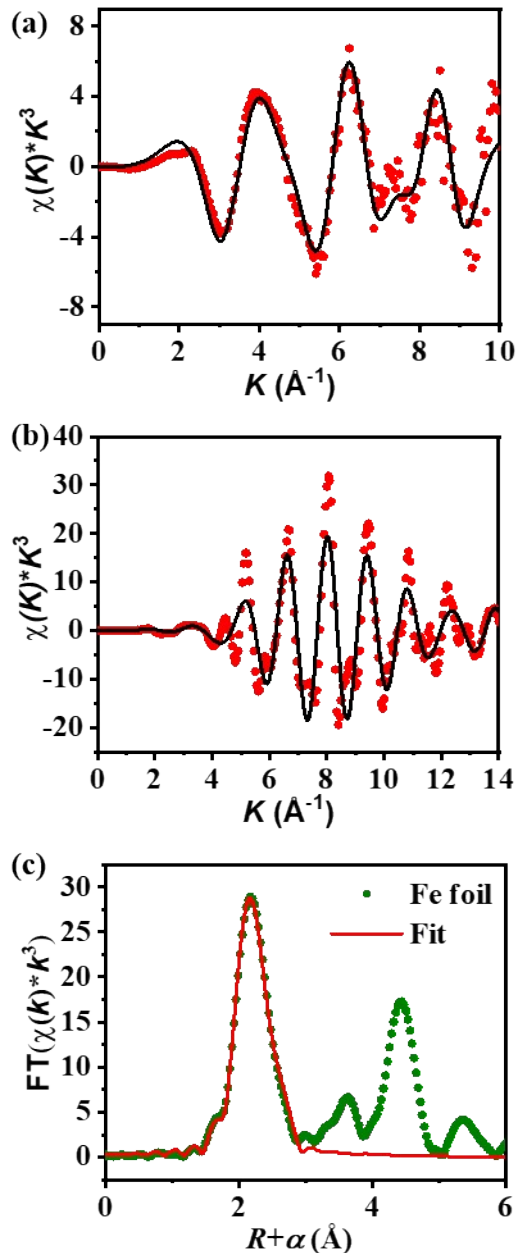


Figure S26. Fe K-edge EXAFS and the curve fit for (a) Fe-ZnMOFS and (b) Fe foil, (c) k^3 -weighted FT-EXAFS (points) and curve fit (line) for Fe-ZnMOFS.

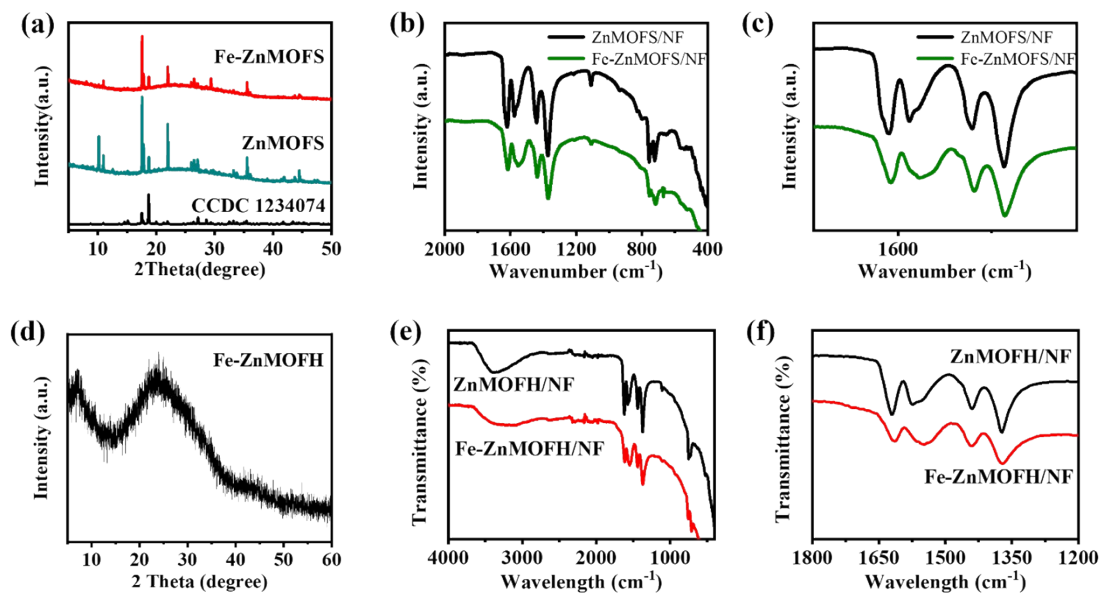


Figure S27. XRD patterns of Fe-ZnMOFS (a) and Fe-ZnMOFH (d). FTIR spectra of Fe-ZnMOFS/NF (b, c) and Fe-ZnMOFH/NF (e, f).

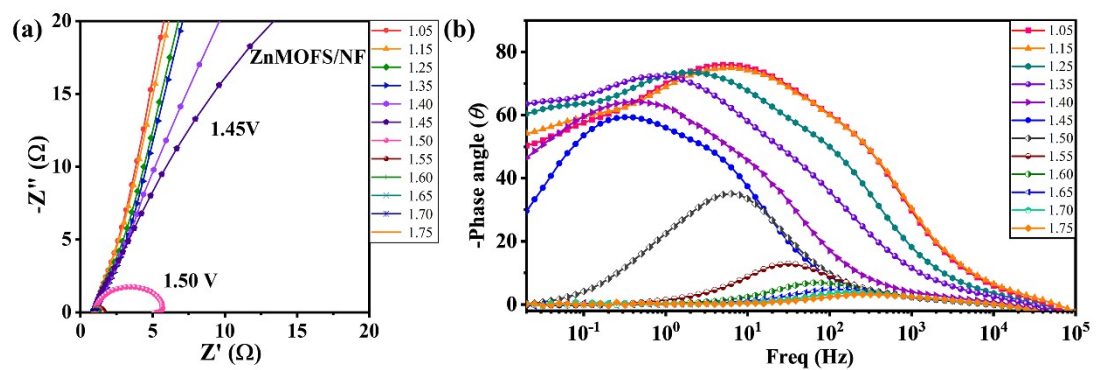


Figure S28. (a) Nyquist plots and (b) Bode plots of ZnMOFS/NF electrode in 1.0 M KOH from 1.05 to 1.75V.

5. Reaction mechanism and decoupling water splitting measurements

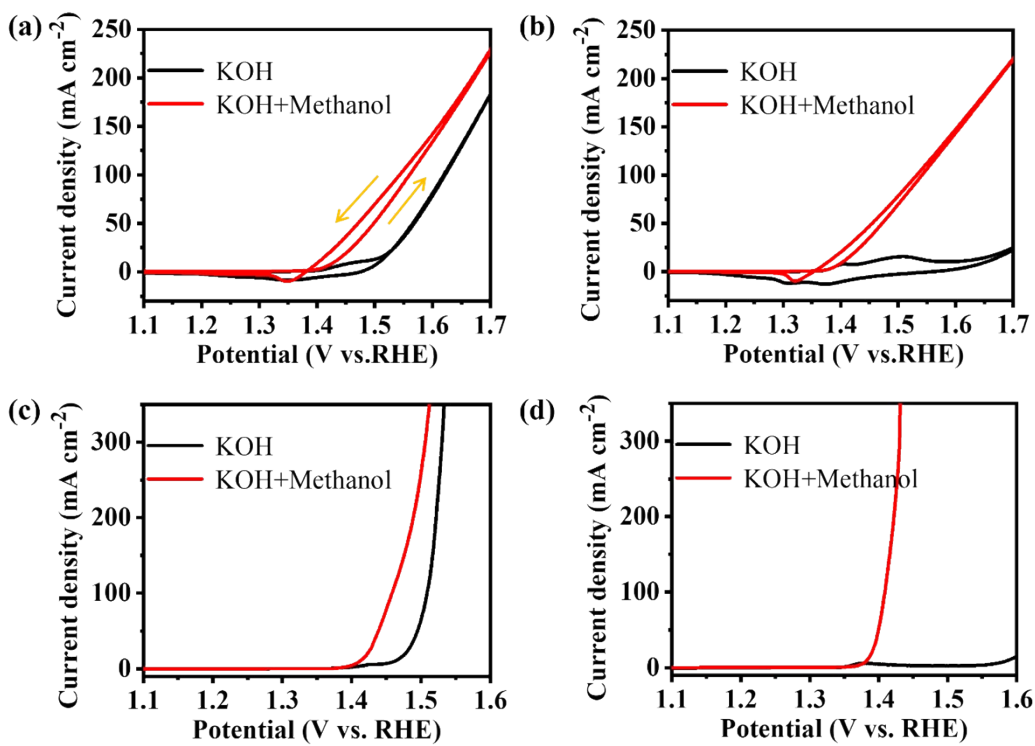


Figure S29. Linear sweep voltammetry curves of (a) Fe-ZnMOFS/NF and (b) ZnMOFS/NF collected in 1M KOH solution and 1M KOH + CH_3OH solution. LSV curves of (c) Fe-ZnMOFS/NF and (d) ZnMOFS/NF with 95% iR compensation.

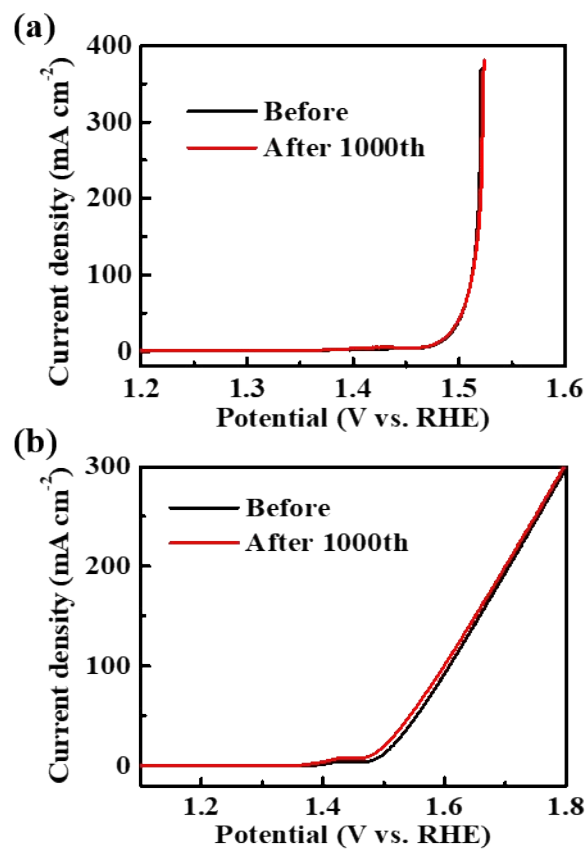


Figure S30. OER polarization curves before and after 1000 cycle CV tests with (a) and without iR compensation (b).

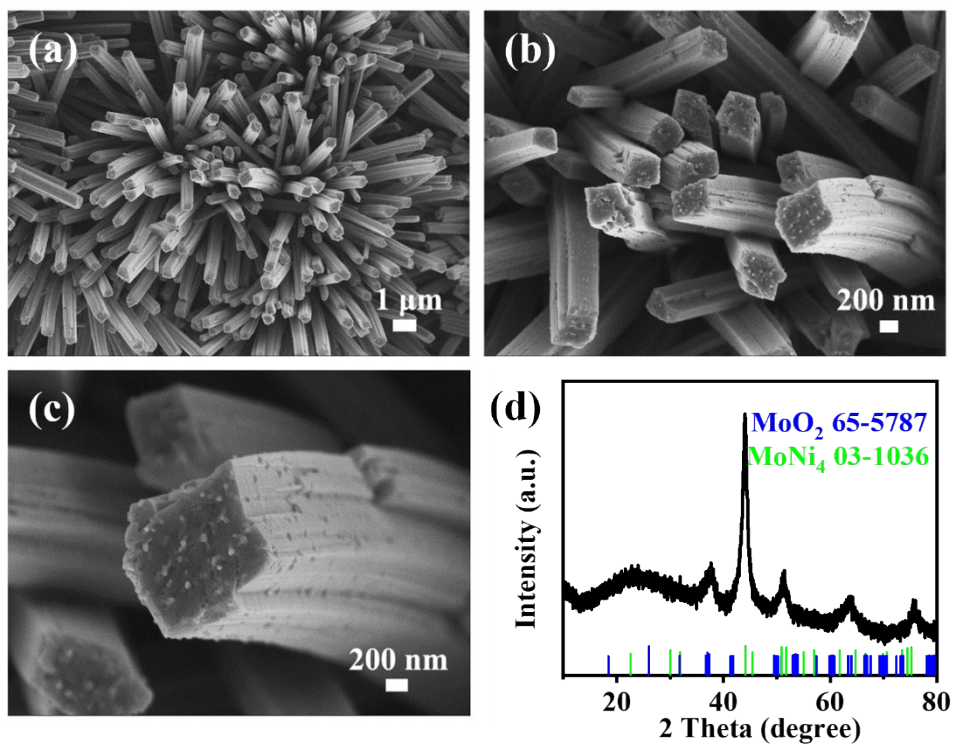


Figure S31. (a-c) SEM images of MoNi₄/MoO₂/NF electrode and (d) XRD patterns of MoNi₄/MoO₂ scrapped from nickel foam.

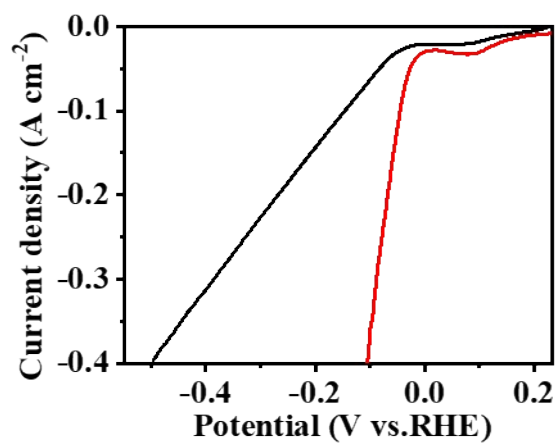


Figure S32. HER polarization curves of $\text{MoNi}_4/\text{MoO}_2/\text{NF}$ electrode toward HER with and without IR compensation.

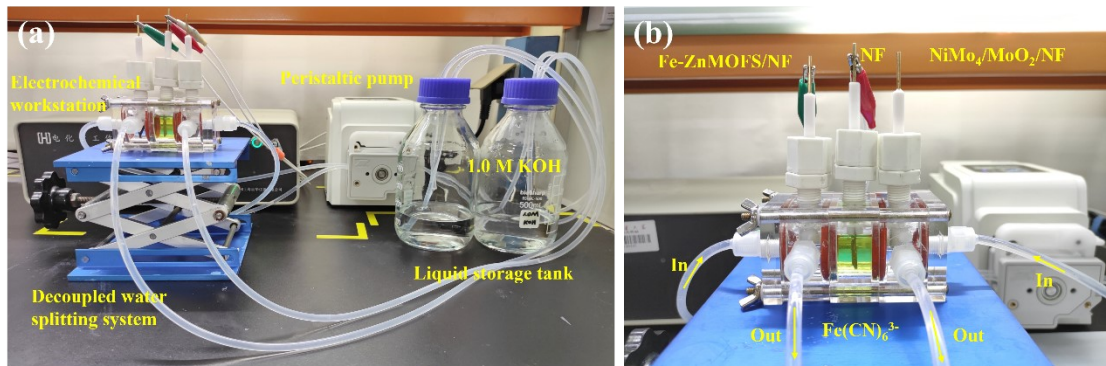


Figure S33. Digital photos of (a) decoupled water splitting system and (b) decoupled electrolysis cell.

6. Table

Table S1. Element contents in diverse Zn based MOFs.

Elements	ZnMOF	ZnMOFH	Fe-ZnMOFH	ZnMOFS	Fe-ZnMOFS
C	51.8	40.4	41.2	43.3	46.7
O	40.3	47.1	46.4	44.8	45.0
Zn	7.9	12.5	6.1	11.9	7.1
Fe			6.3		1.2

Table S2. Fe *K*-edge EXAFS fitting parameters for Fe foil and Fe-ZnMOFS.

Catalyst	Shell	N	R (Å)	σ^2 (Å ²)	ΔE_0 (eV)	R factor
Fe foil	Fe-Fe	8	2.47	0.004	-1.238± 1.34	0.007
	Fe-Fe	6	2.85	0.005		
Fe-ZnMOFS	Fe-O1	6	1.99± 0.01	0.006± 0.001		
	Fe-C	4	3.02± 0.02	0.001± 0.002	2.509± 1.100	0.009
	Fe-O2	4	3.41± 0.03	0.001± 0.002		

O1 and O2 represent the first and second neighbor coordination shell, respectively. N, coordination number; R, the distance between absorber and backscatter atoms; σ^2 , Debye-Waller factor; ΔE_0 , inner potential correction; R factor, the goodness of fit. Amplitude reduction factor S_0^2 was fixed to 0.78 via fitting the FT-EXAFS of Fe foil standard.

Table S3. Oxygen evolution performance comparison of diverse electrocatalysts.

Electrode	Overpotential @10 mA cm ⁻² (mV)	Tafel slope (mV dec ⁻¹)	Stability (h)	Ref.
Fe-ZnMOFS/NF	240	34	800	This work
Triple layer Fe–Co–Ni MOF	254	51.3	48	1
LCN-0.5 HoMS	330	59	10	2
NiFeMOF/G	258	49	10	3
Ni _{1.5} Sn@triMPO ₄	240	45.2	10	4
(Ni ₂ Co ₁) _{1-x} Fe _x -MOF-NF Fe _{0.4} Co _{0.6} Se ₂	258 270	41.3 36	35 24	5 6
Co@CoFe–P NBs	266	26.94	12	7
NiCo _{2-x} Fe _x O ₄ NBs	274	42	25	8
K _{0.8} Na _{0.2} (MgMnFeCoNi)F ₃	314	55	10	9
Co-TiO ₂	332	72	42	10
LaFe _x Ni _{1-x} O ₃	302	50	20	11
LDH-10	286	82	6	12
Ni _{0.5} Cu _{0.75} /C	400	80	~ 5.6	13
LCN-0.5 HoMS	330	59	10	14
CuFe oxide/CF	294	68	600	15
Zn; NiFeO _x H _y	290	28.4	12	16
ZIF-1h-550	231	57	50	17
2D MOF-Fe/Co	238	52	~ 14 h	18
NFN-MOF/NF	240	58.8	30 h at 250 mA cm ⁻²	19
Co _x Fe _{1-x} -MOF-74	280	56	12	20
CoOx–BPQDs	360	58.5	2	21

Table S4. The fitted parameters of Fe-ZnMOFS/NF electrode at different potentials.

E/V	R _s (Ω)	R _{ct} (Ω)	CPE	
			Y ₀ ($\Omega^{-1} \text{ cm}^{-2} \text{ s}^n$)	α
1.05	0.58	5.71*10 ⁵	3.6*10 ⁻³	0.76
1.15	0.58	2.05*10 ⁵	6.2*10 ⁻³	0.76
1.25	0.57	1.64*10 ⁹	10*10 ⁻³	0.76
1.35	0.56	1.20*10 ⁹	2.1*10 ⁻²	0.76
1.40	0.55	8.58*10 ²	5.9*10 ⁻²	0.83
1.45	0.54	32.86	7.8*10 ⁻²	0.88
1.50	0.54	1.32	6.7*10 ⁻²	0.92
1.55	0.55	0.31	6.1*10 ⁻²	0.91
1.60	0.56	0.16	6.3*10 ⁻²	0.88
1.65	0.57	0.11	7.4*10 ⁻²	0.85
1.70	0.56	0.09	8.8*10 ⁻²	0.81
1.75	0.58	0.07	5.0*10 ⁻²	0.88

7. References

1. F. Shahbazi Farahani, M. S. Rahmanifar, A. Noori, M. F. El-Kady, N. Hassani, M. Neek-Amal, R. B. Kaner and M. F. Mousavi, *J. Am. Chem. Soc.*, 2022, **144**, 3411-3428.
2. H. Wang, J. Qi, N. Yang, W. Cui, J. Wang, Q. Li, Q. Zhang, X. Yu, L. Gu, J. Li, R. Yu, K. Huang, S. Song, S. Feng and D. Wang, *Angew. Chem. Int. Ed.*, 2020, **59**, 19691-19695.
3. Y. Wang, B. Liu, X. Shen, H. Arandiyani, T. Zhao, Y. Li, M. Garbrecht, Z. Su, L. Han, A. Tricoli and C. Zhao, *Adv. Energy Mater.*, 2021, **11**, 2003759.
4. S. Li, Z. Li, R. Ma, C. Gao, L. Liu, L. Hu, J. Zhu, T. Sun, Y. Tang, D. Liu and J. Wang, *Angew. Chem. Int. Ed.*, 2021, **60**, 3773-3780.
5. Q. Qian, Y. Li, Y. Liu, L. Yu and G. Zhang, *Adv. Mater.*, 2019, **31**, 1901139.
6. J.-Y. Zhang, Y. Yan, B. Mei, R. Qi, T. He, Z. Wang, W. Fang, S. Zaman, Y. Su, S. Ding and B. Y. Xia, *Energy Environ. Sci.*, 2021, **14**, 365-373.
7. Y. Zhao, N. Dongfang, C. A. Triana, C. Huang, R. Erni, W. Wan, J. Li, D. Stoian, L. Pan, P. Zhang, J. Lan, M. Iannuzzi and G. R. Patzke, *Energy Environ. Sci.*, 2022, **15**, 727-739.
8. Y. Huang, S. L. Zhang, X. F. Lu, Z.-P. Wu, D. Luan and X. W. Lou, *Angew. Chem. Int. Ed.*, 2021, **60**, 11841-11846.
9. T. Wang, H. Chen, Z. Yang, J. Liang and S. Dai, *J. Am. Chem. Soc.*, 2020, **142**, 4550-4554.
10. C. Liu, J. Qian, Y. Ye, H. Zhou, C.-J. Sun, C. Sheehan, Z. Zhang, G. Wan, Y.-S. Liu, J. Guo, S. Li, H. Shin, S. Hwang, T. B. Gunnoe, W. A. Goddard and S. Zhang, *Nat. Catal.*, 2021, **4**, 36-45.
11. P. Zhang, X. Sheng, X. Chen, Z. Fang, J. Jiang, M. Wang, F. Li, L. Fan, Y. Ren, B. Zhang, B. J. J. Timmer, M. S. G. Ahlquist and L. Sun, *Angew. Chem. Int. Ed.*, 2019, **58**, 9155-9159.
12. C.-X. Zhao, B.-Q. Li, M. Zhao, J.-N. Liu, L.-D. Zhao, X. Chen and Q. Zhang, *Energy Environ. Sci.*, 2020, **13**, 1711-1716.
13. M. A. Ahsan, A. R. Puente Santiago, Y. Hong, N. Zhang, M. Cano, E. Rodriguez-Castellon, L. Echegoyen, S. T. Sreenivasan and J. C. Noveron, *J. Am. Chem. Soc.*, 2020, **142**, 14688-14701.
14. H. Wang, J. Qi, N. Yang, W. Cui, J. Wang, Q. Li, Q. Zhang, X. Yu, L. Gu and J. Li, *Angew. Chem. Int. Ed.*, 2020, **59**, 19691-19695.
15. H. Yang and X. Wang, *Adv. Mater.*, 2019, **31**, 1800743.
16. S. Y. Lim, S. Park, S. W. Im, H. Ha, H. Seo and K. T. Nam, *ACS Catal.*, 2020, **10**, 235-244.
17. L. Zhang, C. Lu, F. Ye, R. Pang, Y. Liu, Z. Wu, Z. Shao, Z. Sun and L. Hu, *Adv. Mater.*, 2021, **33**, 2007523.
18. K. Ge, S. Sun, Y. Zhao, K. Yang, S. Wang, Z. Zhang, J. Cao, Y. Yang, Y. Zhang, M. Pan and L. Zhu, *Angew. Chem. Int. Ed.*, 2021, **60**, 12097-12102.
19. D. Senthil Raja, X.-F. Chuah and S.-Y. Lu, *Adv. Energy Mater.*, 2018, **8**, 1801065.
20. X. Zhao, B. Pattengale, D. Fan, Z. Zou, Y. Zhao, J. Du, J. Huang and C. Xu, *ACS Energy Lett.*, 2018, **3**, 2520-2526.
21. M. Batmunkh, M. Myekhlai, A. S. Bati, S. Sahlos, A. D. Slattery, T. M. Benedetti, V. R. Gonçales, C. T. Gibson, J. J. Gooding and R. D. Tilley, *J. Mater. Chem. A*, 2019, **7**, 12974-12978.